NUMERICAL SIMULATION OF HOT BUOYANT SUPPLY AIR JET IN A ROOM WITH DIFFERENT OUTLETS

Shobha Lata Sinha

Mechanical Engineering Department, National Institute of Technology, Raipur, C.G., India.
E-mail:shobha_sinha1@rediffmail.com

ABSTRACT

In this investigation control-volume method has been used for simulating the indoor air flow using Lam-Bremhorst low-Reynolds-number k-ε turbulence model. The flow is considered to be steady, two-dimensional and the Boussinesq's approximation has been used for the buoyancy term. The resulting non-linear system of momentum, energy, turbulence kinetic energy and its dissipation equations have been solved on a non-uniform grid by SIMPLE algorithm due to Patankar and SIMPLEC algorithm due to Doormaal et al.. The Power law scheme has been used to discretise the convective/diffusion terms.

The distributions of velocity, temperature, turbulent kinetic energy, and dissipation of kinetic energy in the room have been presented for Reynolds number of $7\times 10^{3}$and for Grashof number up to 10^{7} ($\Delta T = 10^{0}C$) for different locations of inlet and outlet. The inlet air is assumed to be at higher temperature than the walls. It has been observed that flow pattern changes considerably as Gr increases.

Keywords : Turbulent flow, Low Reynolds number k - ε model, Room airflows, Buoyant flow, Coanda effect, Occupied zone, Comfort.

1. INTRODUCTION

It has been observed that from computational perspective the airflows in rooms are very complex. In reality, at reasonable ventilation rates, the flow is fully turbulent in supply ducts, HVAC inlets/outlets and downstream of the edges of the obstacles. Elsewhere the flow is more likely to be weakly turbulent and time unsteady with a wide range of large to small scale flow structures where the molecular transport is important. In the context of heating (or cooling in warm climates), these flows are buoyant, and in some cases, buoyancy drives the mean flow motion. The presence of walls creates so called near wall effects, where the turbulent transport is significantly influenced by a solid surface. Away from the supply air outlet, the velocities and the turbulent kinetic energy decrease, leading to re-laminarization of the flow in some cases. In practical applications, the obstructions within the room create geometrical complexity. In reality, most airflows are inherently three-dimensional, buoyant and unsteady. Due to these characteristics the airflows in room present a great challenge for the available numerical codes and models.

Although India has the tropical weather, even than some part of the country near mountains are very cold. In those part, the constructed houses require ventilation with heating for the human comfort. In this paper, the effect of air-conditioning with heating at different locations of outlet has been discussed for the turbulent flow.

2. REVIEW

The need of precise determination of airflow pattern and temperature distribution in a room was realized at first by air conditioning engineers so as to provide comfort condition of temperature, relative humidity and air velocity throughout the occupied zone. Accordingly the research on thermal comfort and room air movement started at ASHVE/ U. S., Bureau of Mines laboratory in Pittsburgh, which was founded in 1919. CFD was initiated around 1930. The concept of turbulence was introduced into calculation of room airflow after 1970. Yoshikawa and Yamaguchi[1], presented calculation of two-dimensional high Reynolds number flows in room using one equation model. In the same year Nielsen[2] also developed a calculation procedure based on stream function-vorticity approach for predicting two-dimensional flow pattern in a ventilated room using two equation (k-$\in$) model. Thereafter Nomura *et al*.[3], Sakamoto *et al.* [4] calculated three-dimensional forced and natural convection flows using the k-$\in$ turbulence model with the MAC method and compared the results with model experiments.

Most of the room-airflow programs currently in use are based on the numerical technique developed at Imperial College by Patankar and Spalding[5]. This involves control volume method for the conservative form of equations discretised over staggered control volumes using primitive variables. Nielsen *et al*. [6] used a finite-volume method

for the solution of two-dimensional equations for the conservation of mass, momentum and energy with the k-$\in$ turbulence model including the effect of buoyancy. This solution procedure was then extended by Gosman *et al*. [7] for solving three-dimensional isothermal flow in ventilated rooms. Slot ventilated enclosures for various positions of slots have been investigated by Timmon *et al*. [8].

Kato *et al*. [9] extended their earlier work to study the locally balanced supply and exhaust flow with a flow obstacle along with the experimental verification of the numerically predicted results. Chen *et al*. [10] investigated the indoor air quality and thermal comfort in an office under six kinds of air distributions for summer cooling conditions. Baker *et al*. [11] and William *et al*. [12] have carried out CFD modeling for three-dimensional turbulent flow and compared it with bench mark solutions. Murakami *et al*. [13] and Kato *et al*. [14] studied the room airflow distribution with and without buoyancy using k-$\in$, *ASM, DSM* and *EVM* models. Chen and Jiang[15] reviewed the role of k-$\in$ turbulence model for the prediction of room air movement.

3. ASSUMPTIONS USED IN MODELING

Numerical modeling for the airflow is based on the following assumptions:

1. Presence of heat and pollution sources have not been considered.
2. Physical properties such as density, conductivity etc. are assumed to be constant.
3. Only two-dimensional flow has been considered as the inlet and outlet are considered to be extended throughout the width of the room.
4. The flow is considered to be steady, turbulent and incompressible under Boussinesq's approximation.

4. PROBLEM FORMULATION

The airflow and temperature distribution during air-conditioning with heating in a model room have been investigated. The inlet and outlet are on opposite walls and extend along the full width of the room making the flow essentially two-dimensional; obstructions within the room are not considered for the sake of simplicity. Heat sources inside the room are not considered. The configuration of two-dimensional model room of 6m length and 3m height is shown in Figs 2 and 5 where hot air at temperature $\overline{T_o}$ enters with uniform velocity $\overline{U_0}$ while the wall temperature is kept at $\overline{T_w}$. The inlet velocity $\overline{U_0}$ and inlet opening W_1 are taken as characteristic velocity and length respectively. The difference between wall temperature $\overline{T_w}$ and inlet temperature $\overline{T_o}$ is used as a reference for non-dimensionalization of temperature. The following dimensionless variables are introduced to non-dimensionalize the Reynolds averaged form of Navier Stokes equations:

$$u^* = \frac{\bar{u}}{\bar{U}_o}, v^* = \frac{\bar{v}}{\bar{U}_o}, x^* = \frac{x}{W_1}, y^* = \frac{y}{W_1}, p^* = \frac{\bar{p}}{\rho \bar{U}_o^{\,2}}, T^* = \frac{\bar{T} - \bar{T}_w}{\bar{T}o - \bar{T}w}$$

$$t^* = \frac{t}{\frac{W_1}{U_o}}, k^* = \frac{k}{\bar{U}_o^{\,2}}, \varepsilon^* = \frac{\varepsilon}{\frac{\bar{U}_o^{\,3}}{W_1}}, \mu_t^{\,*} = \frac{\mu_t}{\mu}, \ \mathrm{Pr} = \frac{\nu}{\alpha}, \quad Gr = \frac{g\beta(T_o - Tw)W_1^3}{\nu^2}, \ R_e = \frac{U_0 W_1}{\nu}$$

where Pr, Re and Gr are the Prandtl number, Reynolds number and Grashof number respectively.

Pr is taken as 0.7 throughout the computation.

The resulting mean conservation equations in non-dimensional form can be expressed in the following general form (the superscript * and overscore have been dropped for brevity):

$$\frac{\partial(\rho\phi)}{\partial t} = \frac{\partial}{\partial x}(\Gamma_\phi \frac{\partial \phi}{\partial x} - \rho u \phi) + \frac{\partial}{\partial y}(\Gamma_\phi \frac{\partial \phi}{\partial y} - \rho v \phi) + S_\phi$$

Table 1 gives the details of variables ϕ, Γ_φ and source term ($S\phi$) for various conservation equations.

Table1: Notations for Governing Equations in Cartesian Co-ordinates for Turbulent Flow

Equation	ϕ	Γ_ϕ	S_ϕ
Continuity	1	0	0
u-momentum	u	$\frac{1}{\mathrm{Re}}+\frac{\mu_t}{\mathrm{Re}}$	$-\frac{\partial p}{\partial x}+\frac{\partial}{\partial x}(\Gamma_\phi\frac{\partial u}{\partial x})+\frac{\partial}{\partial y}(\Gamma_\phi\frac{\partial v}{\partial x})$
v-momentum	v	$\frac{1}{\mathrm{Re}}+\frac{\mu_t}{\mathrm{Re}}$	$-\frac{\partial p}{\partial y}+\frac{\partial}{\partial x}(\Gamma_\phi\frac{\partial u}{\partial y})+\frac{\partial}{\partial y}(\Gamma_\phi\frac{\partial v}{\partial y})+\frac{Gr}{\mathrm{Re}^2}T$
Turbulence Energy	k	$\frac{1}{\mathrm{Re}}+\frac{\mu_t}{\sigma_k\,\mathrm{Re}}$	$G_k-\rho\varepsilon-G_b$
Dissipation Energy Rate	$\in$	$\frac{1}{\mathrm{Re}}+\frac{\mu_t}{\sigma_\varepsilon\,\mathrm{Re}}$	$\frac{\varepsilon}{k}(f_1C_1G_k-C_2f_2\rho\varepsilon+C_3G_b)$
Energy	T	$\frac{1}{\mathrm{Re}\,\mathrm{Pr}}+\frac{\mu_t}{\mathrm{Re}\,\mathrm{Pr}_t}$	0

$$\mu_t=\mathrm{Re}\frac{C_\mu f_\mu k^2}{\varepsilon},G_b=\frac{Gr}{\mathrm{Re}^3}\frac{\mu_t}{\sigma_t}\frac{\partial T}{\partial y},G_k=\frac{\mu_t}{\mathrm{Re}}\left(2\left(\frac{\partial u}{\partial x}\right)^2+2\left(\frac{\partial v}{\partial y}\right)^2+\left(\frac{\partial u}{\partial y}+\frac{\partial v}{\partial x}\right)^2\right)$$

5. NEAR WALL TREATMENT IN TRANSPORT EQUATION BASED MODELS

The k-$\in$ turbulence model suggested by Launder and Spalding [16] is not applicable in the vicinity of the solid walls where Reynolds number is small. In the low-Re version of k-$\in$ model, the damping of the turbulence near a solid surface due to molecular viscosity is simulated through the use of damping functions multiplying various terms of the transport equations. These damping functions (f_1, f_2, f_μ) and model constants (C_1, C_2, C_3, C_μ) for a low Re k-$\in$ turbulence model suggested by Lam and Bramhorst [17] are as follows:

$$f_\mu=[1-\exp(-0.0165\,\mathrm{Re}_k)]^2(1+\frac{20.5}{\mathrm{Re}_t}),\ f_1=1+\left(\ \frac{0.05}{f_\mu}\ \right)^3$$

$$f_2=1-\exp(-\mathrm{Re}_t^{\,2}),\mathrm{Re}_t=\frac{\mathrm{Re}\,k^2}{\varepsilon},\mathrm{Re}_k=\mathrm{Re}\,k^{\frac{1}{2}}y_p\ ,\mathrm{Re}=\frac{U_oW_1}{\nu}$$

$$C_\mu=0.09,C_1=1.44,C_2=1.92,C_3=1.44,\sigma_k=1.0,\sigma_\varepsilon=1.3,\mathrm{Pr}_t=0.9$$

where Re_t and Re_k are the Reynolds number based on turbulent quantities and distances from the wall (y_p) respectively. In order to predict near wall characteristics Lam-Bremhorst model has been used throughout the computational work.

6. THE GEOMETRY AND BOUNDARY CONDITIONS

A rectangular room 6m long and 3m high has been considered. The air movement in the room has been analyzed for different values of Re and Gr. The room layout has been shown in Figure2 and 5. The boundary conditions are as follows.

At the left and right walls, ceiling and floor

$$u = 0, v = 0, T = 0, k = 0, \varepsilon = \frac{2k}{\mathrm{Re}\, y_p^{\,2}}$$

At the inlet

$$u = 1, v = 0, T = 1, k = 0.005, \varepsilon = \frac{k^{1.5}}{W_1}$$

At the outlet

Neumann conditions have been set for the flow variables at outlet. The outlet velocity profile is iteratively adjusted to satisfy overall mass conservation equation and,

$$\frac{\partial \phi}{\partial n} = 0$$

where n is the direction normal to the outflow boundary.

7. NUMERICAL SOLUTION PROCEDURE

The governing equations have been solved by using a staggered grid system for the velocity components. These equations are discretised using a control volume method. A Power law scheme is used for the discretization of the convective and diffusion terms in the equations. The numerical scheme used herein is based on SIMPLE algorithm due to Patankar[5] and SIMPLEC due to Doormaal et al.[18]. Starting with an initial guess for velocity and pressure distribution, the u and v momentum equations are solved for all the control volumes. The velocity distribution may not satisfy the mass conservation equation for each control volume since the guessed values of pressure and velocity may not be correct. The pressure and velocities are therefore iteratively corrected so as to satisfy the mass conservation equation in each control volume. To complete an iteration k, ε and T equations are solved successively. The TDMA is used to obtain solutions of discretised linear algebraic equations. Iteration and under-relaxation are used to resolve non-linearity. Relaxation factors are 0.5, 0.5, 0.8, 0.4, 0.4 and 0.5 for u, v, p, k, ε and T respectively. The turbulent viscosity is under -relaxed by a factor of 0.5. Converged solution is deemed to have been achieved and iterations are terminated when all the absolute residuals (normalized) are less than 10^{-5}. The solutions were obtained for various grids and found to be grid independent. The numerical solutions were compared with benchmark experimental results reported by Nielsen [19]. The height (H), length (L) and width (W) of the test room are 2m, 6m and 2m respectively. The inlet and outlet dimensions are 0.112m and 0.32m respectively and extend throughout the width of the room.

Fig. 1 shows a comparison of the horizontal velocity (U) and turbulent intensity (I = 0.909 k^0.5) at two vertical cross-sections. These experimental results are at the central plane where the two-dimensional numerical predictions can be compared with the measured data of three-dimensional case. The agreement is observed to be very good. A grid of 100×80 in x and y directions respectively has been used. The grid spacing was uniformly expanded away from the wall according to a power law formulation with a power of 1.3-1.4.

Fine grids are needed near the walls to capture the transition of flow from turbulent to laminar -like near the wall. The total number of grids in x and y directions were chosen so as to ensure that y^+ was of the order of 0.5 for the first grid point adjacent to the wall so that very steep gradients of k and near the wall can be resolved. This criterion is a requirement for the low Re number model used in the present work.

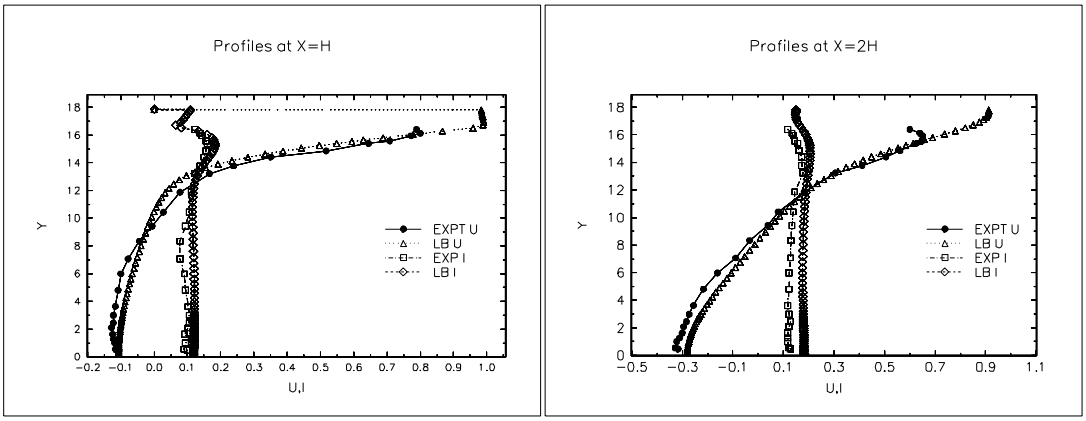

Figure 1: Velocity Profile (U) and Turbulent Intensity(I) at two different sections

8. RESULTS & DISCUSSIONS

In this paper, the effects of air-conditioning and heating at different locations of inlet jet and outlet with different values of Gr have been discussed. Table 2 & 3 show the supply airflow rate, air change rate, temperature rise corresponding to Re / Gr in the air-conditioned room.

Table 2: Supply airflow rate (SR) and air change rate (ACH)

Opening Size(m)	Re	Velo.(m/s)	SR(m^3/s)	ACH(/hr)
0.2	7000	0.56	0.112	22.4

Table 3: Temperature Rise Corresponding to Gr

Opening Size(m)	Gr	$\Delta T(^\circ C)$
0.2	10^5	0.1
0.2	10^6	1.0
0.2	10^7	10.0

8.1 Case 1: Inlet near the floor and outlet adjacent to the ceiling on opposite walls (Re=7000)

In this case, inlet of width 0.2m is provided on the left wall at 0.5m above the floor level and outlet of width 0.5m is provided 2.5m above the floor as shown in Fig. 2.

The streamline plots are shown in Figs. 3 (a-c) for Re=7000 and three values of Gr, namely 10^7, 2.5×10^7 and 5×10^7 respectively. At Gr $= 10^7$, the main stream of warm fluid enters through the inlet, attaches with the floor at $x \approx 0.9$m due to Coanda effect, moves along the floor, rises up near the right wall and then moves along it before leaving. One small recirculating cell is observed just below the inlet at the bottom-left corner due to Coanda effect and a large recirculating cell has been observed above the main stream. As Gr increases, the point of attachment shifts towards the left wall. The intensity of upper recirculating zone increases with the increase of Gr. The extent of recirculation zone on the left-bottom corner reduces with the increase of Gr.

As Gr increases to 2.5×10^7 (Fig. 3b), the main stream attaches with the floor at $x \approx 0.8$m, moves along the floor and rises up suddenly due to the buoyancy, attaches with the ceiling at $x \approx$ 2.7m and moves along the ceiling towards exit. This gives rise to one more recirculation cell in the

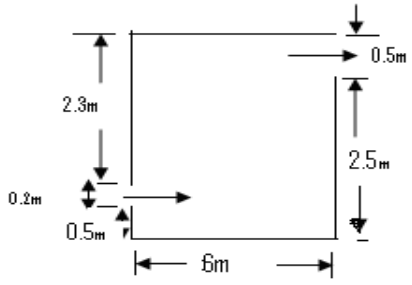

Figure 2: Outlet and inlet locations of the room (Case 1)

right part of the room and the upper recirculation cell gets squeezed towards the left side of the main stream. The intensity and extent of the left side recirculation cell decrease and those of right side recirculation cell increases as Gr increases. At Gr $= 5\times10^7$ (Fig. 3c), buoyancy force becomes so large that the main stream does not attach with the floor, instead it attaches with the left wall, rises along it and moves along the ceiling towards the exit. The left recirculation cell completely vanishes. The intensity and extent of recirculation cell below the main stream increase.

The isotherms for this case are shown in Figs. 3 (d-f). The temperature variation is significant along the primary flow. The temperature profile near the floor is similar to that of wall jet. Temperature is uniform in the upper recirculatory region at Gr $= 10^7$. As Gr increases to 2.5×10^7, the temperature variation is like the wall jet near the floor and other isotherms follow the main stream which attaches with the ceiling. At Gr $= 5\times10^7$, the temperature variation is very steep along the left wall and the main stream, and is observed to be uniform in most of the room.

The variation of the Nusselt number, along the walls, floor and ceiling is shown in Figs. 4 (a-b) for Gr $= 10^7$. The Nusselt number has been found to be maximum near the lower lip of the inlet, that is, at the beginning of recirculation cell due to Coanda effect on the left wall. In this zone, heat transfer rate is large due to the presence of the shear layer and the entrainment. On the right wall, the Nusselt number is larger in comparison to that at the left wall since the heated main stream moves along it for Gr $= 10^7$.

The highest value of the Nusselt number has been observed at the point of attachment on the floor at x ≈ 0.8m because of large temperature gradient near the stagnation point. As the main stream moves along the floor, the Nusselt number reduces in the wall jet due to increasing thickness of thermal boundary layer. The flow is from the right to the left along the ceiling. There will be a thermal boundary layer on the ceiling. The Nusselt number on the ceiling decreases from right to left as the thickness of boundary layer increases. The Nusselt number increases on both the walls, ceiling and floor as Gr increases.

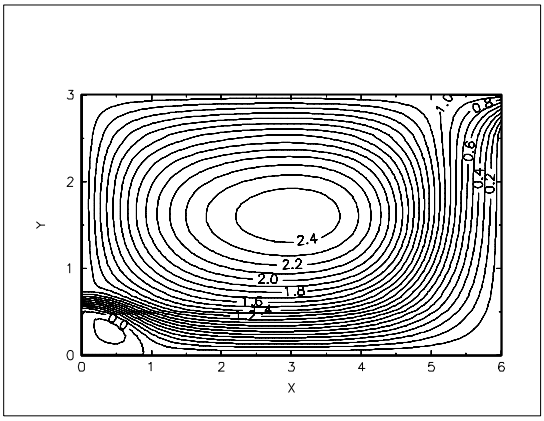

(a) SC (Gr=10^7)

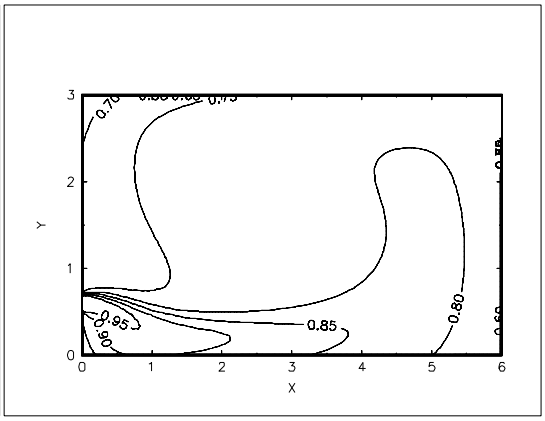

(d) TC (Gr=10^7)

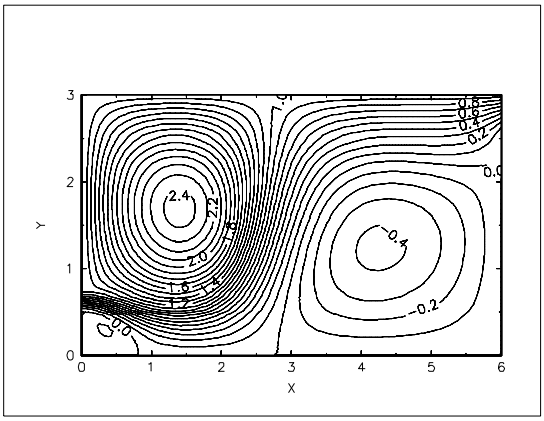

(b) SC (Gr=2.5 $\times 10^7$)

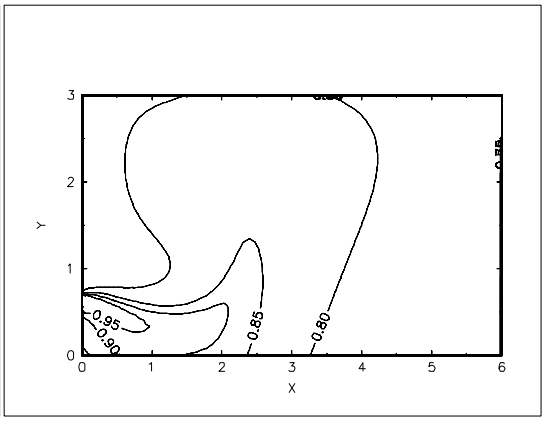

(e) TC (Gr=2.5 $\times 10^7$)

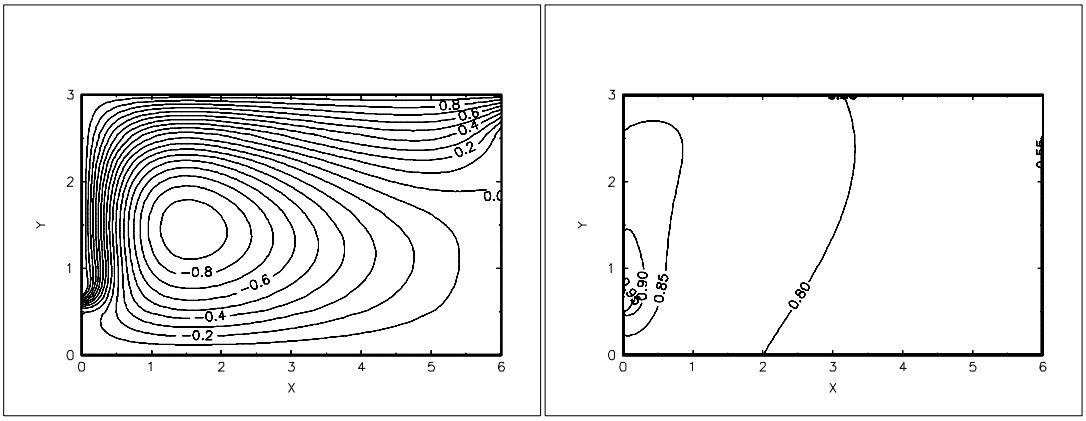

(c) SC (Gr=5 $\times 10^7$) (f) TC (Gr=5 $\times 10^7$)

Figure 3: Contours of streamlines Re=7000 and ACH=22.4/hr (Case 1).

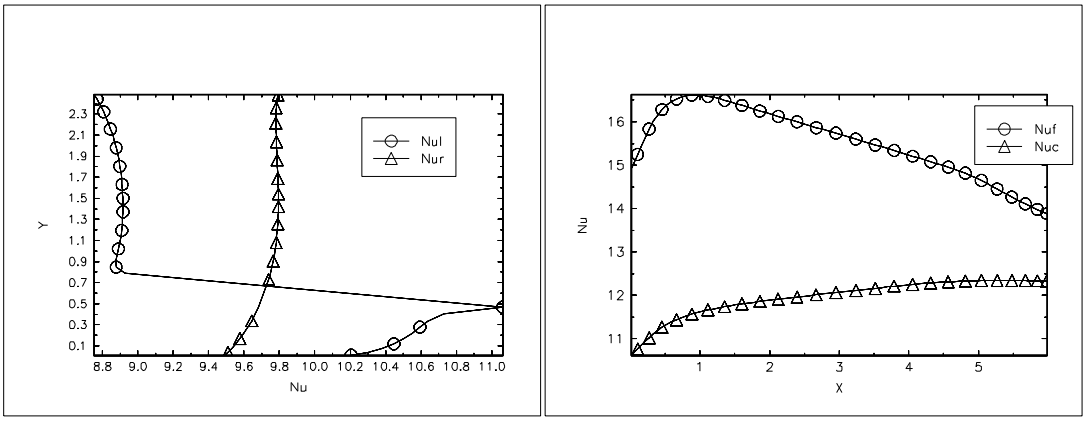

(a) NUV (Gr=10^7) (b) NUH (Gr=10^7)

Figure 4: Variation of Nusselt number along the walls, floor and ceiling for Re=7000 and ACH=22.4/hr(Case 1).

8.2 **Case 2: Inlet and outlet both near the floor on opposite walls (Re=7000)**

In this case, the inlet and the outlet both of width 0.2m are provided on the left and right walls at height of 0.5m above the floor level as shown in Fig. 5.

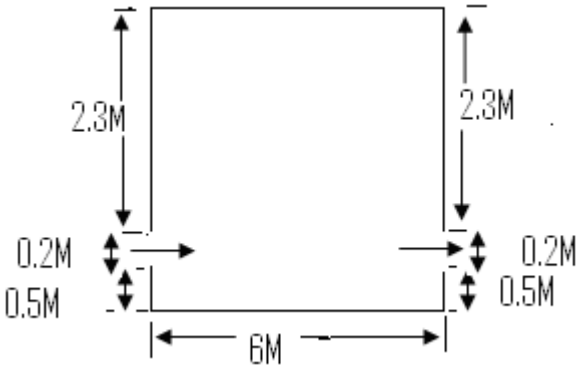

Figure 5: Outlet and inlet locations of the room (Case 2)

The streamline plots are shown in Figs. 6 (a-c) for Re=7000 at three values of Gr, namely, 10^6, 10^7 and 2.5×10^7. The main stream enters through the inlet, attaches with the floor at $x \approx 1$m due to Coanda effect, moves along the floor and slightly rises up before leaving.

One small recirculating cell just below the inlet at the bottom-left corner and one large recirculating cell above the main stream have been observed. The magnitude of upper recirculating zone increases with the increase of Gr. The extent of small recirculating cell reduces with the increase of Gr. At $Gr = 10^7$ (Fig. 6 b), the streamline labelled '1.0' attaches with the ceiling instead of the right wall and a part of the main stream rises towards the ceiling and then drops down along the warm right wall before leaving. This is due to the strong effect of buoyancy. At $Gr = 2.5 \times 10^7$ (Fig. 6 c), the main stream directly rises up along the left wall after entering the room, moves along the ceiling and the right wall subsequently before leaving. The Coanda effect disappears due to the prominent effect of buoyancy. Only one recirculation cell has been observed below the main stream.

The isotherms for this case are shown in Figs. 6 (d-f). The isotherms reveal profiles similar to those for free jet near the inlet with a small thermal potential core of uniform temperature, wall jet after attachment and uniform temperature distribution in the circulation region. The temperature drops at faster rate in stream-wise direction at higher values of Gr. The temperature distribution becomes steeper near the left wall and uniform in most of the room at higher values of Gr.

The variation of the Nusselt number along the walls, floor and ceiling is shown in Figs. 7 (a-f).

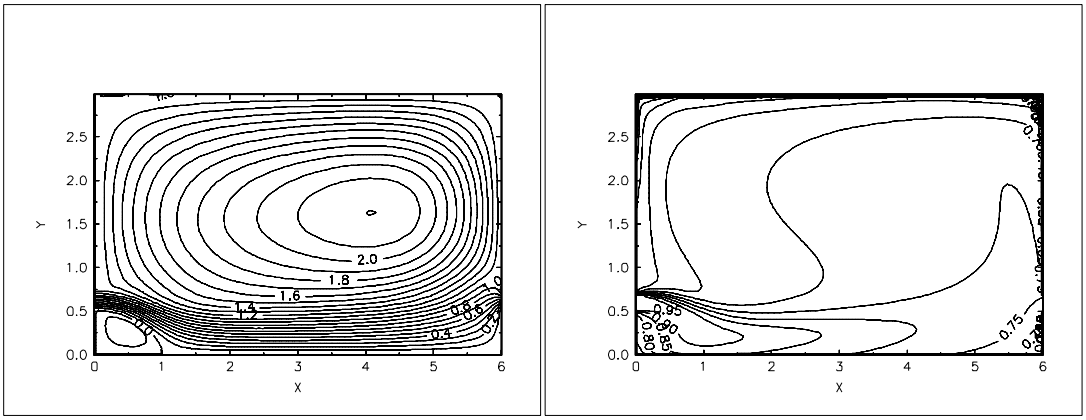

(a) SC ($Gr=10^6$) (d) TC ($Gr=10^6$)

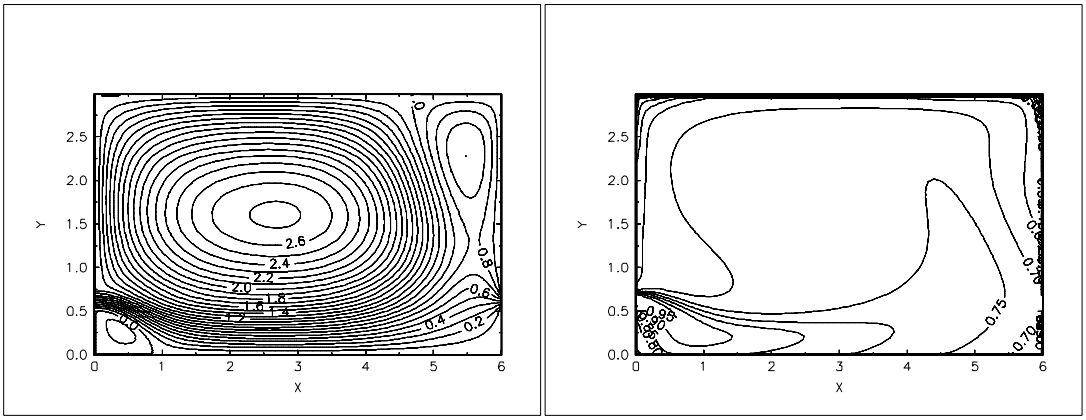

(b) SC ($Gr=10^7$)(e) TC ($Gr=10^7$)

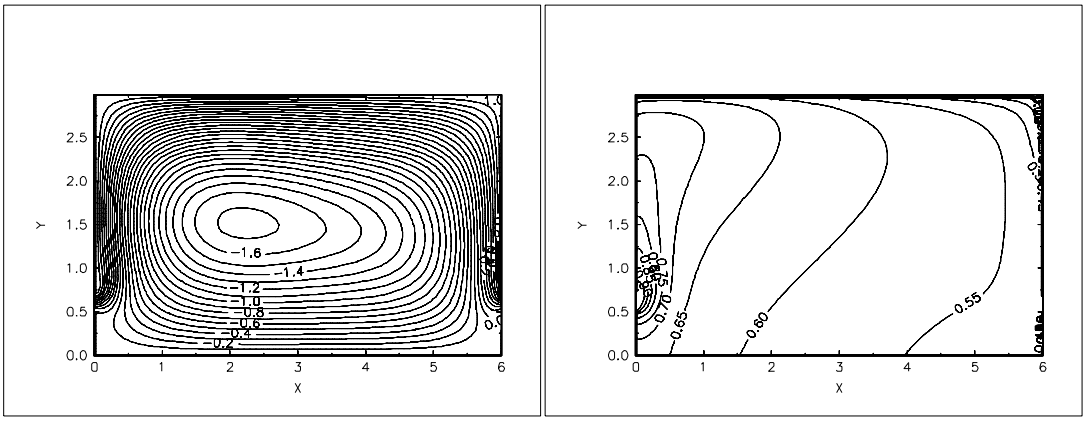

(c) SC (Gr=2.5 $\times 10^7$) (f) TC (Gr=2.5 $\times 10^7$)

Figure 6: Contours of streamlines and temperatures for Re=7000 and ACH=22.4/hr (Case2).

The Nusselt number has been found to be maximum ($\approx$ 10.0) near the lower lip of the inlet. It has the high values in recirculation region near the left wall. In this zone, heat transfer rate is large due to the shear layer and the entrainment. The Nusselt number is observed to be larger on the right wall than that on the left wall for Gr $< 2.5 \times 10^7$. At Gr $= 2.5 \times 10^7$, the Nusselt number

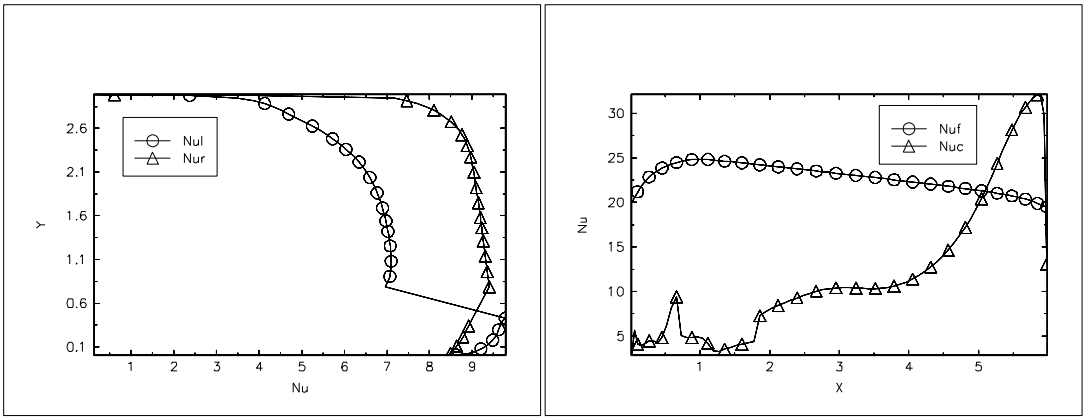

(a) NUV (Gr=10^6) (d) NUH (Gr=10^6)

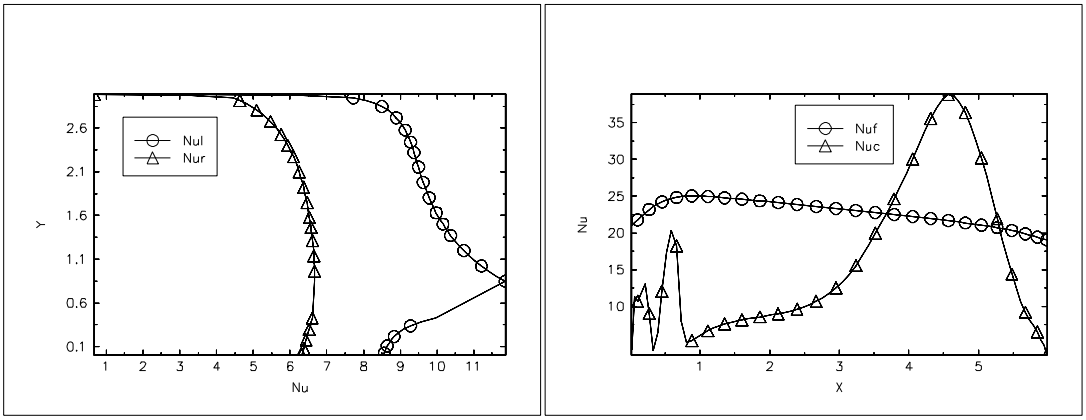

(b) NUV (Gr=10^7) (e) NUH (Gr=10^7)

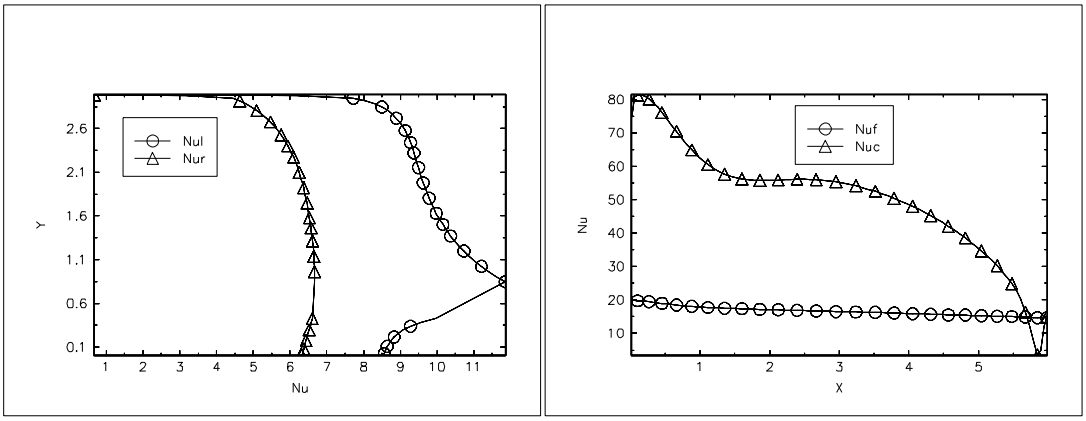

(c) NUV (Gr=2.5 $\times 10^7$) (f) NUH (Gr=2.5 $\times 10^7$)

Figure 7: Variation of Nusselt number along the walls, floor and ceiling for Re=7000 and ACH=22.4/hr (Case 2).

increases drastically on the left wall due to the sudden change in the streamline pattern. The highest value of the Nusselt number has been observed at the point of attachment on the floor at x ≈ 1m because of large temperature gradient near the stagnation point. As the main stream moves along the floor, the Nusselt number reduces slightly in the wall jet due to increasing thickness of boundary layer. The flow is from the right to the left along the ceiling. There will be a thermal boundary layer on the ceiling. The Nusselt number on the ceiling decreases from right to left as the thickness of boundary layer increases. The Nusselt number increases on both the walls, ceiling and floor as Gr increases. The Nusselt number on the ceiling for Gr = 10^7, increases upto x ≈ 4.5m due to the high entrainment and then it reduces near the right wall. The Nusselt number on the floor for Gr = 2.5×10^7, is smaller than that for lower values of Gr and remains almost constant throughout the floor. The Nusselt number on the ceiling decreases from left to right as the main stream moves along it at Gr = 2.5×10^7. The temperature difference and velocity both are large on left part of the ceiling, which gives rise to larger value of the Nusselt number.

9. CONCLUSIONS

In both of the cases, recirculation zones have been observed on either side of the main stream. In Case 1, where the inlet is near the floor and outlet is adjacent to the ceiling on the opposite wall, the fluid directly rises after entry through the inlet at $Gr/Re^2 \approx 0.5$. In Case 2 where both, the inlet and the outlet are 0.5m above the floor respectively, fluid directly rises after entering in the room at $Gr/Re^2 \approx 0.2$.

The temperature variation is found to be significant along the primary flow. The primary flow exhibits a thermal potential core. Temperature is found to be almost uniform in the recirculation zones. Sharp temperature gradients have been observed near the walls. The isotherm essentially follow the path of the main stream. The length of thermal potential core reduces as Gr increases.

The maximum value of Nusselt number occurs at the point of attachment where the stagnation of flow occurs along the walls, ceiling and floor depending upon the path of the main stream, Coanda effect and effect of buoyancy.

10. NOTATIONS

G	Acceleration due to gravity
G_k , G_b	Generation due to TKE and buoyancy respectively
TKE	Turbulent kinetic energy
P	Pressure
Pr_t	Turbulent Prandtl number
SC,TC	Streamline and Temperature Contour
T	Temperature
u	Velocity in x-direction
u_τ	Friction velocity(τ_w/ρ)
v	Vertical velocity
x, y	Linear dimensions on abscissa and ordinate
y_p	Minimum distance between the wall and adjacent grid
y^+	Non-dimensionalized y distance (yu_τ/ν)

Greek Symbols

α	Thermal diffusivity
Γ_φ	Effective diffusivity
β	Coefficient of thermal expansion
ΔT	Difference between inlet and wall temperature
μ	Dynamic Viscosity
μ_t	Turbulent viscosity
ρ	Mass density
ν	Kinematic viscosity
τ_w	Shear stress at the wall
	TKE dissipation rate
σ_k , σ	Empirical constants of turbulence for turbulent energy and energy dissipation rate
φ	Dependent variable

11. REFERENCES

[1]. Yashikava, A. and Yamaguchi, K., Numerical Analysis of Indoor Air Flows, Japanese Society of Heating-Cooling Air Conditioning and Sanitary Engineering (J.S.H.A.S.E.) in Japanese, 1974, 48.

[2]. Nielsen, P. V., Flows in Air Conditioned Room, Ph D Thesis, Technical University of Denmark, 1974.

[3]. Nomura, T., Matsuo, Y., Kaizuka, M., Sakamoto, Y. and Endo, K., Numerical Study of Room Air Distribution-Part 3, Architectural Institution of Japan (in Japanese), 1975, 238.

[4]. Sakamoto, Y., Matsuo, Y., Nomura, T. and Kamata, M., Numerical Prediction of Three-Dimensional Thermal Convection by means of 2-Equation Turbulence Model, Proceedings of Annual Meeting of Architectural Institution of Japan (in Japanese), 1978.

[5]. Patankar, S. V., Numerical Heat Transfer and Fluid Flow, McGraw Hill, Washington, 1980.

[6]. Nielsen, P.V., Restivo, A. and Whitelaw, J.H., Buoyancy Affected Flows in Ventilated Rooms, Numerical Heat Transfer, 1979, 2, 115-127.

[7]. Gosman, A.D., Nielsen, P.V., Restio, A. and Whitelaw, J.H., The Flow Properties of Rooms with Small Ventilation Openings, Journal of Fluid Engineering, Sept.1980, 102, 316-323

[8]. Timmons, M.B. and Albright, L.D., Experimental and Numerical Study of Air Movement in Slot Ventilated Enclosures, ASHRAE Trans., Part 1, 1980, 221-240.

[9]. Kato, S., Murakami, S. and Nagano, S., Numerical Study of Diffusion in a Room with a Locally Balanced Supply Exhaust Air Flow Rate System, ASHRAE Trans., Part 1, 1992, 98, 218-238.

[10]. Chen, Q., Moser, A. and Suter, P., A Numerical Study of Indoor Air Quality and Thermal Comfort under Six Kinds of Air Diffusion, ASHRAE Trans., Part 1, 1992, 98, 203-217.

[11]. Baker, A.J., Williams, P.T. and Kelso, R. M., Numerical Calculation of Room Air Motion-Part 1: Math, Physics and CFD Modeling, ASHRAE Trans., Part 1, 1994, 100, 514-530.

[12]. Williams, P.T., Baker, A.J. and Kelso, R. M., Numerical Calculation of Room Air Motion-Part 3: Three-dimensional, CFD Simulation of a Full Scale Room Air Experiment, ASHRAE Trans., Part 1, 1994, 100, 549-564.

[13]. Murakami, S., Kato, S. and Ooka, R., Comparison of Numerical Predictions of Horizontal Non-isothermal Jet in a Room with Three Turbulence Models- k-$\in$, EVM, ASM and DSM, ASHRAE Trans., Part 2, 1994, 100, 697-704.

[14]. Kato, S., Murakami, S. and Kondo, Y., Numerical Simulation of Two-Dimensional Room Airflow with and without Buoyancy by Means of ASM, ASHRAE Trans., Part 1, 1994, 100, 238-255.

[15]. Chen, Q and Jiang, Z., Significant Questions in Predicting Room Air Motion, ASHRAE Trans., Part 1, 1992, 11, 929-939.

[16]. Launder, B.E. and Spalding, D.B., Mathematical Models of Turbulence, Academic Press, 1972.

[17]. Lam, C.K.G. and Bremhorst, K., A Modified Form of the k-$\in$ Model for Predicting Wall Turbulence, Journal of Fluid Engineering, 1981, 103, 456-460.

[18]. Van Doormal, J.P. and Raithby, G.D., Enhancement of the SIMPLE Method for Predicting Incompressible Fluid Flow, Numerical Heat Transfer, 1984, 7, 147-163.

[19]. Nielsen, P.V., Specification of a Two-Dimensional Test Case, International Energy Agency, Energy Conservation in Buildings and Community Systems, Annexure 20: Air Flow Pattern Within Buildings, 1-15 (November 1990), ISSN 0902-7513 R9040.